THE EFFECT OF THE ADJACENT TOOTH AND RIM ELASTICITY ON FATIGUE BEHAVIOR IN THIN-RIMMED SPUR GEARS

[1]IVAN ČULAR, [2]KREŠIMIR VUČKOVIĆ, [3]ROBERT MAŠOVIĆ, [4]DRAGAN ŽEŽELJ, IVICA GALIĆ

University of Zagreb, Faculty of Mechanical Engineering and Naval Architecture, Croatia
E -mail: [1]ivan.cular@fsb.hr

Abstract: Thin-rimmed gears are often used in industries requiring lightweight components, such as aerospace industries. However, the existing standards and typical simulation methods often induce errors when estimating the bending fatigue life of a gear, such as neglecting the elasticity of the rim and the adjacent tooth effect. In this paper, an already established and experimentally validated computational model is applied to thin-rimmed spur gears to estimate the bending fatigue lives. Moreover, a comparison between various estimation approaches with respect to different bending stress cycles is made. It can be concluded that finite element analysis without considering the adjacent tooth effect overestimates the actual results significantly, while ISO 6336 standard underestimates them, particularly in low-cycle fatigue regions.

Keywords: Thin-rimmed Gear, Bending Fatigue Life, Strain-life Method, Finite Element Analysis, Adjacent Tooth Effect

I. INTRODUCTION

Gears are one of the most commonly employed machine elements for power transmission. Due to their loading, the major principal stress at the tooth root (bending stress) is cyclic or, more specifically, periodic. Hence, fatigue at the tooth root (bending fatigue) may result in tooth breakage and gear failure. In industries that favor lightweight components, such as aerospace industries, webbed gears, also known as thin-rimmed gears, are often employed. In such gears, the rim's elasticity and the often-neglected phenomenon of the adjacent tooth effect [1] significantly affect the bending stress cycle and, consequently, the bending fatigue of a thin-rimmed gear.The existing standards for gear's loading capacity calculation, such as ISO 6336 standard [2], do not account for the elastic deformation of gear teeth as they contact the teeth from the opposite gear, i.e., the standard assumes ideally rigid gear teeth. This effect is particularly interesting in thin-rimmed gears, where elastic deformation due to the lack of material is more significant compared to solid gears (gears without the thin rim). An example of gear contact between the solid and thin-rimmed gear is shown in Figure 1.

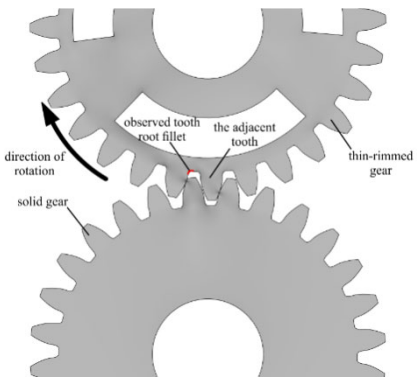


Fig.1. An example of gear contact between the thin-rimmed gear (top) and solid gear (bottom)

In Figure 2, a schematic representation of three nominal bending stress cycles is shown: according to the ISO 6336 standard, according to FEM (finite element method), and according to FEM without consideration of the adjacent tooth and rim elasticity effects.

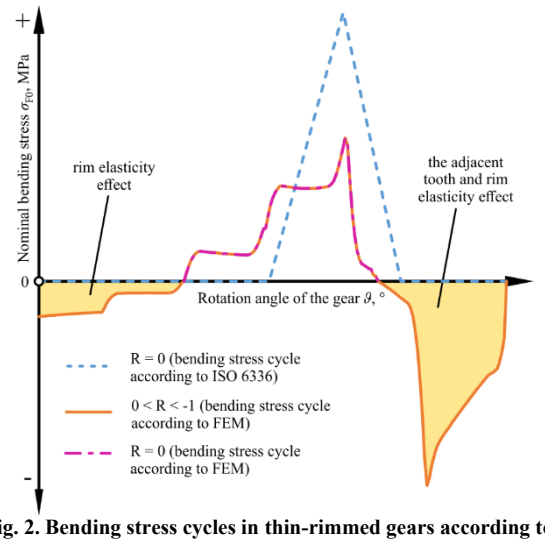


Fig. 2. Bending stress cycles in thin-rimmed gears according to ISO 6336 standard and FEM (with and without consideration of the adjacent tooth and rim elasticity effects)

ISO 6336 standard accounts for the thin-rimmed gears by employing a compensating factor Y_B. However, this only multiplies the maximum tensile stress (blue dashed line in Figure 2). The most accurate bending stress cycle representation is shown by the solid orange line in Figure 2, demonstrating rim elasticity and adjacent tooth effects. However, as previously mentioned, researchers often overlook these effects [1], only focusing on tensile stresses (dashed purple line in Figure 2). This may be because tensile stresses are generally more dangerous than compressive ones regarding material fatigue. Therefore, in this paper, a computational model for bending fatigue life estimation of thin-rimmed gears is proposed. Moreover, from the safety standpoint,

crack initiation instead of complete failure is assumed. In addition, the obtained fatigue lives are compared against the fatigue lives obtained when ISO 6336 [2] stress cycle is employed. This standard does not consider the adjacent tooth effect and tends to overestimate the maximum stresses. Furthermore, the influence of the aforementioned and often overlooked adjacent tooth effect[3]is also investigated. Lastly, it should be noted that the investigation conducted in this paper is based on computational models previously established and experimentally validated by the authors [1, 4 – 6].

II. MATERIALS AND METHODS

2.1. Geometry and Material of the Gear Pair

Geometrical and material parameters of the driving (solid) gear, Z_1, and driven (thin-rimmed) gear, Z_2, are shown in Table 1.

Parameter	Driving (solid) gear, Z_1	Driven (thin-rimmed) gear, Z_2
Number of teeth	28	
Module	3.175 mm	
Profile shift coefficient	0	
Face width	6.35 mm	
Pressure angle of the basic rack	20°	
Tip relief (at tooth tip)	0.013 mm	
Root fillet radius of the basic rack	0 mm	
Addendum of the basic rack	3.334 mm	
Dedendum of the basic rack	4.286 mm	
Tip diameter	95.25 mm	
Center distance	88.9 mm	
Rim thickness/tooth height (addendum + dedendum) ratio	-	0.5 (taken as the lowest recommended value according to [2])
Young's modulus	207 GPa	
Poisson's coefficient	0.33	
Gear material	14NiCrMo 13-4 (AISI 9310)	

Table 1: Geometrical and material parameters of the gear pair

2.2. Numerical Simulation

After establishing the geometry of the gear pair, a finite element model was made within a commercially available program Abaqus [7]. A quasi-static finite element simulation was conducted, meaning that the rotation of the gear pair was separated into fixed and equal increments; within each increment, a static analysis was conducted. The analysis is linear-elastic, and the material is assumed as homogenous and isotropic.

The numerical simulation with boundary conditions is shown in Figure 3. Reference points RP_1 and RP_2 were coupled via kinematic coupling with the inner hub of the solid gear and the thin-rimmed gear, respectively. According to Pehan et al. [8], a plane-stress assumption can be made if the gear's face width is less than six times its module, which is the case in this simulation. Therefore, a 2D numerical simulation was conducted using CPS4 (first-order plane stress) finite elements. The observed tooth root fillet was chosen on the middle tooth on the thin rim (Figure 3), which consists of seven teeth. This tooth was chosen since the rim's elastic deformation will be most pronounced here.

The numerical simulation was separated into two steps:

1) In the first step, contact between the initial pair of teeth was established by applying the torque T on the driving gear and fixing both radial and rotational displacement of the driven gear via reference point RP_2. Only rotational displacement at RP_1 was allowed, while the radial displacement was fixed. Contact was established via normal behavior and hard contact. By assuming adequate lubrication conditions, the effect of friction was not considered here [9 – 11].

2) In the second step, rotational displacement of RP_2 is enabled, and the driven gear rotates by an angle $\vartheta = 77°$ with continuous application of torque T on the driving gear. The time required for the total rotation is 10 seconds, and each increment is taken as 0.05 seconds, i.e., a total of 200 increments are obtained. To investigate both low and high-cycle bending fatigue behavior, torque T was chosen from 100 Nm to 300 Nm, with an interval of 50 Nm. Lastly, convergence analysis was carried out to ensure the accuracy of the results.

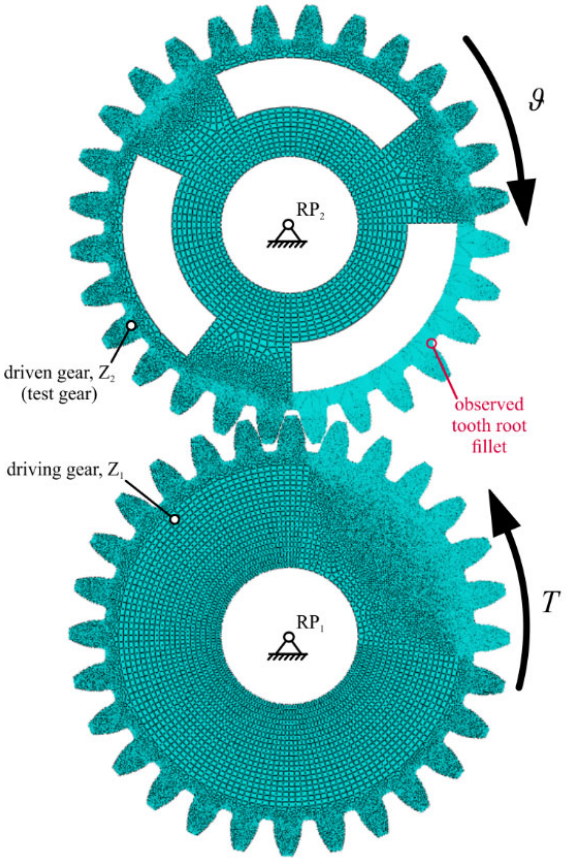


Fig. 3. Finite element simulation with boundary conditions

Once the simulation was completed, a bending stress cycle similar to the one shown in Figure 2 (solid orange line) was obtained for all nodes at the observed tooth root fillet. This is the first type of bending stress cycle used in this paper to investigate the bending fatigue life. The second type of the bending stress cycle investigated in this paper is obtained by only considering the tensile part of the previously obtained cycles (purple dashed line in Figure 2). This is a common error found in literature since many bending fatigue investigations of gears apply a single force on the tooth flank (due to simplicity) or simulate a single contact increment (for example, at the HPSTC – the highest point of single tooth contact). Consequently, only tensile stress is produced at the tooth root, i.e., compressive bending stress due to the rim's elasticity and the adjacent tooth effect are not accounted for.

The third type of bending stress cycle investigated in this paper is according to ISO 6336 calculations. Here, an ideally rigid tooth is assumed, where the effect of the thin rim is accounted for by employing the factor Y_B [2]:

$$Y_B = 1.6 \ln\left(2.242 \frac{1}{m_B}\right) \quad (1)$$

where m_B is the ratio of the rim's thickness (measured from the root diameter to the rim's inner diameter) to the tooth height (addendum + dedendum). Thus, a bending stress cycle similar to the one shown in Figure 2 (blue dashed line) is obtained. It should be noted that the maximum tensile bending stress values obtained by ISO 6336 standard are significantly higher than the ones obtained by the conventional FEM modeling, as demonstrated in Table 2.

Torque T, Nm	σ_{F0} according to ISO 6336, MPa	σ_{F0} according to the FEM, MPa
100	1019	421
150	1529	622
200	2038	821
250	2548	992
300	3057	1117

Table 2: Maximum linear-elastic tensile bending stresses for the thin-rimmed gear

However, ISO 6336 standard does not account for the compressive bending stress portion of the cycle, which modifies both the stress amplitude and the mean stress, consequently affecting bending fatigue lives.

After obtaining three different types of often-employed bending stress cycles, bending fatigue lives are calculated according to the previously established and experimentally validated fatigue model [4 – 6] briefly described in the next section.

2.3. The Fatigue Model

Due to the notch-like behavior of the material at the tooth root, actual stresses and strains might differ from linear elastic ones obtained via FEM or ISO 6336 standard, especially in low-cycle fatigue. Therefore, elastic-plastic correction according to Neuber's rule [12] is first conducted. Hence, actual stresses and strains accounting for localized plasticity effects are obtained.

Then, the strain-life (ε – N) method estimates the required number of cycles for bending fatigue crack initiation. In the absence of actual fatigue data (which is often the case in carburized spur gears due to heterogenous material), the hardness method [13] can be successfully employed. This method can be used to obtain strain-life fatigue properties according to the following equations:

$$\sigma_f^{'} = 425 \cdot \mathrm{HB} + 225 \tag{2}$$

$$\varepsilon_f^{'} = \frac{0.32 \cdot (\mathrm{HB})^2 - 487 \cdot \mathrm{HB} + 191000}{E} \tag{3}$$

$$b = -0.56 \tag{4}$$

$$c = -0.09 \tag{5}$$

where $\sigma_f^{'}$ the fatigue strength coefficient,HB is the Brinell hardness, $\varepsilon_f^{'}$ is the fatigue ductility coefficient, E is Young's modulus,b is the fatigue strength exponent, andc is the fatigue ductility exponent. Moreover, the cyclic strength coefficient K' and cyclic strength exponent n'required for Neuber's correction can also be obtained as follows [14]:

$$K' = \frac{\sigma_f^{'}}{\left(\varepsilon_f^{'}\right)^{n}} \tag{6}$$

$$n' = \frac{b}{c} \tag{7}$$

Geometric parameters of the investigated gear pair are taken from [15], where it is stated that the surface hardness of the thin-rimmed gear is 61 HRC. According to the hardness conversion tables from [16], 61 HRC equals 670 HB. Hence, fatigue properties defined by Eqs. (2-7) can be obtained. It should be noted that the investigated gear is assumed to be carburized and adequately annealed to relax residual stresses. Hence, the effect of residual stresses is not investigated here. Finally, the required number of cycles for bending fatigue crack initiation can be obtained via the strain-life method according to Eq. (8):

$$\varepsilon_a^a = \frac{\sigma_f^{'} - \sigma_m^a - \sigma_{res}}{E} \cdot \left(N_f\right)^b + \varepsilon_f^{'} \cdot \left(N_f\right)^c \tag{8}$$

where ε_a^a is the actual strain amplitude (corrected for elastic-plastic material behavior), N_f is the number of reversals until fatigue failure, σ_m^a is the actual mean stress, and σ_{res} is the residual stress assumed as zero within this investigation. Lastly, it should be mentioned that commercially available software FE-Safe [17] was employed in combination with the FE analysis to facilitate the calculation process.

III. RESULTS AND DISCUSSION

Bending fatigue lives for the aforementioned three types of cycles are shown in Figure 4.

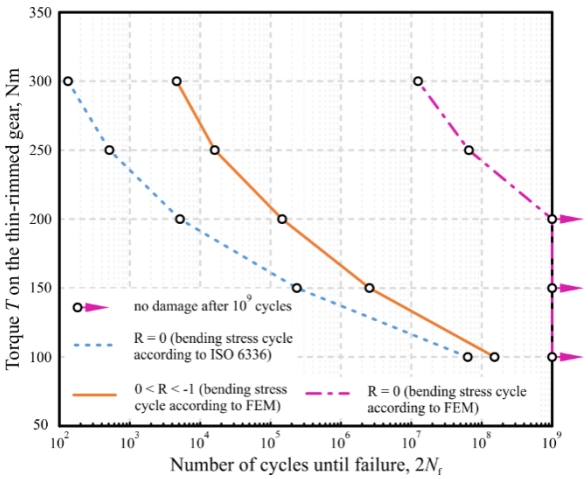


Fig. 4. Estimated bending fatigue lives with respect to three different types of bending stress cycles

According to Figure 4, it can be observed that the ISO 6336 standard provides the most conservative results (blue dashed line). Compared with the most accurate bending stress cycle (represented by the solid orange line), their respective difference in bending fatigue lives gradually increases with load (torque). In other words, the greatest difference is observed in low-cycle fatigue and is gradually lowered towards the high-cycle fatigue region. Even though conservative fatigue estimations are desirable in material fatigue, such estimations can often result in over-dimensioned mechanical components. Hence, more accurate results, such as those obtained by the 0 < R < -1 FEM prediction (solid orange line), should be made.

On the other hand, ignoring the rim's elasticity and the adjacent tooth effect can lead to a dangerous phenomenon of significantly overestimated bending fatigue lives, as shown in Figure 4 by the dashed purple line. It should be noted that 10^9 cycles was chosen as the cut-off point. In other words, no damage criterion was applied if the estimated number of cycles was higher than 109.

Lastly, a few remarks regarding the failure location should also be made. As stated in the introductory part of this paper, surface bending fatigue failure (the most common failure type) is assumed here, i.e., bending fatigue failure occurs at the tooth root fillet. However, ISO 6336 standard assumes a fixed failure location. This location is defined by a fixed angle of 30°, which is the angle between two lines; the first line is the symmetry line of the gear's tooth, and the second line is the line tangent to the tooth root's fillet.

According to the FEM model, the failure location for both types of cycles (with and without considering the rim's elasticity and the adjacent tooth effect) is also on the tooth root fillet, but not precisely at the angle of 30°. Nevertheless, generally speaking, the failure locations for all three types of cycles are in relative agreement.

IV. CONCLUSIONS

In this paper, a numerical model based on a previously validated computational model was proposed to estimate the required number of cycles for bending fatigue crack initiation in thin-rimmed spur gears. Moreover, a comparison was made between bending fatigue lives obtained via the FEM (finite element method) and fatigue lives using ISO 6336 stress cycles. Lastly, the often-overlooked rim's elasticity and adjacent tooth effectswere also explored. The following conclusions can be drawn:
1) Bending fatigue life estimations based on ISO 6336 stress cycles tend to underestimate the actual results significantly. Even though conservative results are desirable in fatigue, they may lead to over-dimensioned mechanical components.
2) Bending fatigue life estimation without accounting for the rim's elasticity and adjacent tooth effects tends to significantly overestimate the actual results, which is particularly dangerous since a false safety assumption is made. Hence, these effects should always be accounted for, particularly in thin-rimmed gears.

Someassumptions of the study should also be mentioned. First, a 2D instead of 3D FE analysis was conducted, somewhat lowering the accuracy of the results. Moreover, the effect of friction was not considered, which typically slightly increases or decreases (depending on the observed gear) maximum tensile stresses. Lastly, the effect of centrifugal force was also not accounted for. Even though this effect is often insignificant in solid spur gears, it might be significant in thin-rimmed gears, particularly above 10 000 rpm. However, since one of the main goals of this paper is the comparison between different types of stress cycles, the abovementioned assumptions are present in all three types of observed cycles, canceling each other out for the most part.

In future work, the effect of various rim thicknesses will be investigated. Moreover, since gears are sometimes additionally surface hardened via processes such as shot penning, bending fatigue cracks tend to initiate below the surface, as demonstrated in previous investigations. Hence, a thin-rim model considering subsurface bending fatigue failure will be established in the future.

REFERENCES

[1] K. Vučković, I. Čular, R. Mašović, I. Galić, and D. Žeželj, "Numerical model for bending fatigue life estimation of carburized spur gears with consideration of the adjacent tooth effect," International Journal of Fatigue, vol. 153, 2021.

[2] ISO 6336, Calculation of Load Capacity of Spur and Helical Gears, 2006.

[3] Franco Concli, Lorenzo Fraccaroli, Lorenzo Maccioni, "Gear Root Bending Strength: A New Multiaxial Approach to Translate the Results of Single Tooth Bending Fatigue Tests to Meshing Gears," Metals, vol. 11, 863, 2021. DOI: 10.3390/met11060863

[4] I. Čular, K. Vučković, S. Glodež, and Z. Tonković, "Computational model for bending fatigue prediction of surface hardened spur gears based on the multilayer method," International Journal of Fatigue, vol. 16.

[5] I. Čular, K. Vučković, I. Galić, and D. Žeželj, "Computational model for bending fatigue life and failure location prediction of surface-hardened running gears," International Journal of Fatigue, vol. 166, 2023.

[6] I. Čular, "Fatigue modeling in surface-hardened spur gears," Doctoral dissertation, University of Zagreb, Faculty of Mechanical Engineering and Naval Architecture, 2022.

[7] Abaqus 6.13, Dassault Systems, 2013.

[8] S. Pehan, T. Hellen, J. Flašker and S. Glodež, "Numerical methods for determining stress intensity factors vs. crack depth in gear tooth roots," International Journal of Fatigue, vol. 19, no. 10, pp. 677-685, 1997. DOI: 10.1016/S0142-1123(97)00101-1

[9] K. Vučković, I. Galić, Ž. Božić and S. Glodež, "Effect of friction in a single-tooth fatigue test," International Journal of Fatigue, vol. 114, pp. 148-158, 2018. DOI: 10.1016/j.ijfatigue.2018.05.005

[10] R. Martins, J. Seabra, A. Brito, C. Seyfert, R. Luther, and A. Igartua, "Friction coefficient in FZG gears lubricated with industrial gear oils: Biodegradable ester vs. mineral oil," Tribology International, vol. 39, no. 6, pp. 512-521, 2006.

[11] B. R. Höhn, K. Michaelis, and A. Doleschel, "Frictional behaviour of synthetic gear lubricants," Tribol. Ser., vol. 39, pp. 759–768, 2001.

[12] H. Neuber, "Theory of Stress Concentration for Shear Strained Prismatical Bodies with Arbitrary Non-Linear Stress Strain Law," Journal of Applied Mechanics, vol. 28, no. 4, pp. 544-550, 1961.

[13] M. L. Roessle and A. Fatemi, "Strain-Controlled Fatigue Properties of Steels and Some Simple Approximations," International Journal of Fatigue, vol. 22, no. 6, pp. 495-511, 2000. DOI: 10.1016/S0142-1123(00)00026-8

[14] R. Stephens, A. Fatemi, R. Stephens, and H. Fuchs, Metal Fatigue in Engineering, 2nd Edition, John Wiley & Sons, inc., 2001.

[15] R. Handschuh, T. Krantz, B. Lerch, and C. Burke, "Low-Cycle Bending Fatigue of AISI 9310 Steel Spur Gears," NASA/TM-2007-214914, 2007.

[16] E 140 – 02, Standard Hardness Conversion Tables for Metals Relationship Among Brinell Hardness, Vickers Hardness, Rockwell Hardness, Superficial Hardness, Knoop Hardness, and Scleroscope Hardness, 2002.

[17] FE-SAFE Version 6.5, User guide, Safe technology limited, 2014.

★★★